Three-Dimensional Viscous Flow Solutions with a Vorticity-Stream Function Formulation

R. L. Davis* and J. E. Carter†
United Technologies Research Center, East Hartford, Connecticut
and
M. Hafez‡
University of California, Davis, California

A three-dimensional streamlike function/vorticity transport procedure has been developed for the analysis of two- and three-dimensional steady, inviscid and viscous external flows. Special care has been taken to incorporate interacting boundary-layer concepts into this Navier-Stokes procedure in order to take advantage of the features that interacting boundary-layer techniques offer but retain the generality of Navier-Stokes methods. Numerical techniques have been applied to the present formulation that honor the elliptic nature of the flow in the inviscid region and the parabolic nature in the viscous part of the flow. An implicit, successive line relaxation technique is used to solve two sets of streamlike function/vorticity transport equations for the streamwise and crossflow components of the flow. Solutions are presented for a series of model problems that demonstrate that this Navier-Stokes technique is capable of yielding accurate solutions that simultaneously capture the details of the inviscid and viscous flow regions.

Nomenclature

C_{f_x} = axial component of skin friction
C_{f_z} = spanwise component of skin friction
L = reference length
p = static pressure
Re = freestream reference Reynolds number
u = axial (x) component of velocity
v = normal (y) component of velocity
V = velocity vector
V_∞ = freestream speed
w = spanwise (z) component of velocity
x = axial Cartesian coordinate
y = normal Cartesian coordinate
z = spanwise Cartesian coordinate
ν = kinematic viscosity coefficient
θ = stream function in z,y plane
ψ = stream function in x,y plane
ω = vorticity vector
ω_x = vorticity component in the axial (x) direction
ω_y = vorticity component in the normal (y) direction
ω_z = vorticity component in the spanwise (z) direction

Introduction

THE analysis of complex three-dimensional flow is a problem that continues to challenge fluid dynamicists. Although significant progress has been made in this area for three-dimensional inviscid flows, considerable development is still needed for the accurate solution of three-dimensional viscous flows. The step from inviscid to viscous flows is a major one as small length scale phenomena are introduced that require significant advances in present day computational fluid dynamics methodology to obtain an accurate, efficient procedure that properly analyzes the flow. The analysis of three-dimensional viscous flows has been performed with either boundary-layer or Navier-Stokes techniques.

Although boundary-layer procedures are quite efficient, the boundary-layer equations, when solved subject to a prescribed pressure distribution, have a singularity at separation and, therefore, cannot be used in this manner for the calculation of separated flows. Interacting Boundary-Layer Theory (IBLT) in which the boundary-layer equations are solved iteratively with an inviscid solution procedure have been developed by a number of investigators for two-dimensional separated flows (e.g., see Refs. 1-4). Only recently have efforts been initiated to extend interacting boundary-layer theory to three-dimensional flows.[5-7] IBLT procedures are very efficient techniques for solving strongly interacting viscous and inviscid flows, since the respective flow regions are solved independently. By breaking the flow field up in this manner, efficient solvers can be matched to each region. Increases in configuration complexity for either internal or external flows result in a displacement surface that becomes increasingly difficult to track, and hence interacting boundary-layer techniques can become very tedious to implement.

An alternative approach, which is currently pursued by most of the computational fluids technical community, is to solve the Navier-Stokes equations numerically. In principal, this approach is the most exact since these are the fundamental governing equations of fluid motion. However, high Reynolds number viscous flows, which generally characterize aerodynamic flows that are of practical importance, are well known to generate multiple length scale phenomena that render most numerical techniques for the Navier-Stokes equations inefficient when attempts are made to obtain accurate solutions. Most, if not nearly all, of the developments of these numerical procedures have been driven by the inviscid flow solvers with little emphasis placed on the incorporation of viscous flow considerations derived from either attached or strongly interacting boundary-layer methodologies. Clearly, an effort is needed to build on what has been learned about high Reynolds number interacting flows in the development of new formula-

Presented as Paper 87-0601 at the AIAA 25th Aerospace Sciences Meeting, Reno, NV, Jan. 12-15, 1987; received Feb. 2, 1987; revision received Aug. 15, 1988.

*Senior Research Engineer. Member AIAA.
†Manager, Computational Mathematics and Fluid Dynamics. Member AIAA.
‡Professor. Member AIAA.

tions and numerical methods for the Navier-Stokes equations. Some work in this area has been initiated in the development of efficient generalized viscous-inviscid solution procedures that can be eventually extended to three-dimensional flows. Noteworthy among these efforts is the forcing function concept introduced by Steger and van Dalsem[8] and the pseudo-function concept approach of Whitfield.[9] Although the details of these procedures differ substantially, they both impose the viscous prediction of a vorticity distribution on the inviscid flow to account for the viscous-inviscid interaction phenomena.

The overall goal of the present investigation[10] has been to incorporate interacting boundary-layer concepts into a Navier-Stokes procedure in order to take advantage of the features that interacting boundary-layer techniques offer but retain the generality and flexibility of Navier-Stokes procedures. This approach has been pursued by casting the Navier-Stokes equations into a streamlike function and vorticity transport form for the solution of three-dimensional incompressible, external flows. By formulating the equations in this manner, the solution procedure can take advantage of the fact that at high Reynolds number, the flow can be broken into an inviscid region, where a central differenced Poisson equation set is used for the description of the elliptic nature of the flow, and into a viscous region, where one-sided windward differenced vorticity transport equations are used to model the parabolic nature of the flow. Interaction between the inviscid and viscous flows occurs through a vorticity source term in the Poisson equations.

Significant work has previously taken place in the development of numerical procedures to solve the two-dimensional stream function/vorticity transport equations. Examples of this work include Werle and Bernstein,[11] Briley,[12] Ghia and Davis,[13] and the recent work of Halim and Hafez[14] on which much of the present work is based. For three-dimensional internal flows, Hamed and Abdallah[15] have initiated extensions of vorticity/streamlike function concepts to three dimensions for flow within ducts. Aziz and Hellums,[16] Wong and Reizes,[17] Aregbesola and Burley,[18] and Yang and Camarero[19] have developed solution procedures for duct flows using a vector potential methodology. These formulations differ considerably from that developed in the present investigation. In particular, the present formulation is a relatively simple subset of the vector potential equations specifically for external flows. This Navier-Stokes formulation will be shown to have many of the characteristics of a generalized three-dimensional viscous-inviscid interaction procedure without the use of boundary-layer approximations or explicit coupling procedures.

Analysis

In this section, the governing equations and boundary conditions for the three-dimensional streamlike function/vorticity transport formulation of the incompressible, steady Navier-Stokes equations are presented. A major focal point of this research effort has been to use solution techniques that take advantage of the elliptic nature of the outer, inviscid flow simultaneously interacting with the parabolic-like nature of the viscous flow region.

Governing Equations

The nondimensional form of the Navier-Stokes equations for laminar, incompressible steady flow are given by

$$\nabla \cdot V = 0 \tag{1}$$

for the conservation of mass and

$$V \cdot \nabla V = -\nabla p + \frac{1}{Re} \nabla^2 V \tag{2}$$

for the conservation of momentum. In this formulation, the velocity is nondimensionalized by the freestream speed V_∞, the pressure by twice the freestream dynamic pressure $\rho_\infty V_\infty^2$, and all lengths by a reference length L. The kinematic coefficient of viscosity ν, which is constant for incompressible flow, is represented in terms of the Reynolds number given by $Re = V_\infty L/\nu$. Vorticity is introduced into this formulation by taking the curl of Eq. (2) which, with the usual definition of vorticity

$$\omega = \nabla \times V \tag{3}$$

leads to the vorticity transport equation given by

$$V \cdot \nabla \omega = \omega \cdot \nabla V + (1/Re)\ \nabla^2 \omega \tag{4}$$

Lighthill[20,21] has presented an extended discussion to show that vorticity is a very useful quantity that can be used to describe most fluid dynamic phenomena. It is particularly attractive for describing low-speed flows since vorticity is produced only at solid surfaces due to viscosity and, hence, is nonzero only in viscous regions. The transport of vorticity described in Eq. (4) is influenced by three dominant physical effects that are represented by the terms in this equation. Solid boundaries act as a distributed source (or sink) of vorticity, which is diffused and convected away from the surface by the $\nabla^2\omega/Re$ and $V \cdot \nabla\omega$ terms, respectively. In two-dimensional flows, these terms are equal whereas in three-dimensional flow, which is the focus of the present study, there is an additional term $\omega \cdot \nabla V$, which represents the stretching of the vortex lines due to the velocity field. Equations (1), (3), and (4) represent a system of seven equations in six unknowns, those being the three components of velocity and vorticity. One of these equations must be dropped in order to obtain a balanced system. The continuity equation, given in Eq. (1), is retained so as to maintain conservation of mass. Furthermore, the vorticity definition, Eq. (3), is retained so as to ensure the conservation of vorticity or, as it sometimes is referred to, the solenoidality condition, obtained by taking the divergence of Eq. (3) to give

$$\nabla \cdot \omega = 0 \tag{5}$$

Since vorticity is conserved according to Eqs. (3) and (5), only two of the vorticity transport equations are required to define the entire vorticity field so that one transport equation can be dropped to yield a balanced set of six equations for the six unknowns. In the present study, which has been limited to boundary-layer-like flows including separation, there are two dominant components of vorticity. Hence, the transport equations for these components have been included, and the transport equation for the third component of vorticity about an axis normal to the surface has been dropped. This is not an approximation, but it is a special formulation suitable only for a particular class of external flow problems.

Two functions can be introduced that automatically ensure that mass conservation is satisfied. These functions ψ and θ, both of which are like a stream function for two-dimensional flow, are related to the velocity components through the following definitions

$$u = \frac{\partial \psi}{\partial y} \tag{6}$$

$$v = -\frac{\partial \psi}{\partial x} - \frac{\partial \theta}{\partial z} \tag{7}$$

$$w = \frac{\partial \theta}{\partial y} \tag{8}$$

This relationship between ψ and θ is not unique in satisfying the continuity equation. However, it is a simple procedure that has been found to work very well in the present study. The coordinates x, y, z and velocity components in these respective

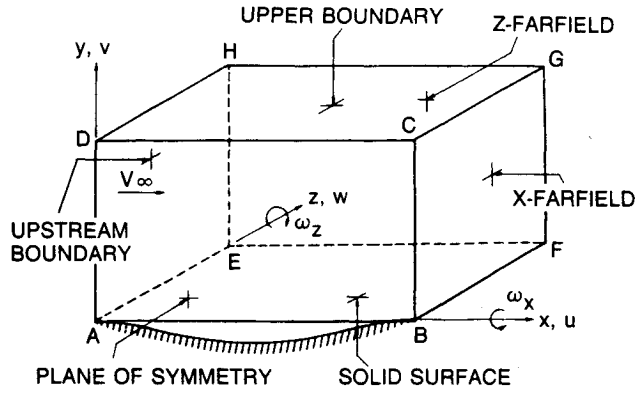

Fig. 1 Computational region around localized symmetric disturbance on flat plate.

directions have been expressed in Eqs. (6–8) in a Cartesian system as shown in the schematic diagram in Fig. 1. The principal reason that these functions have been introduced is to obtain second-order equations for the inviscid portion of the flow, which are well known to be computationally simpler to solve than the first-order Euler equations, which are obtained from Eqs. (1) and (2) for an infinite Reynolds number.

The overall set of governing equations, expressed in terms of the Cartesian coordinates and notation shown in Fig. 1, can now be summarized. The transport equations governing the principal vorticity components ω_z and ω_x, defined by

$$\omega_z = \frac{\partial v}{\partial x} - \frac{\partial u}{\partial y}, \quad \omega_x = \frac{\partial w}{\partial y} - \frac{\partial v}{\partial z} \tag{9}$$

are given by

$$\frac{\partial \psi}{\partial y}\frac{\partial \omega_z}{\partial x} - \left(\frac{\partial \psi}{\partial x} + \frac{\partial \theta}{\partial z}\right)\frac{\partial \omega_z}{\partial y} + \frac{\partial \theta}{\partial y}\frac{\partial \omega_z}{\partial z} - \omega_x\frac{\partial w}{\partial x} - \omega_z\frac{\partial w}{\partial z} - \left(\frac{\partial u}{\partial z} - \frac{\partial w}{\partial x}\right)\frac{\partial w}{\partial y} - \frac{1}{Re}\left(\frac{\partial^2 \omega_z}{\partial x^2} + \frac{\partial^2 \omega_z}{\partial y^2} + \frac{\partial^2 \omega_z}{\partial z^2}\right) = 0 \tag{10}$$

$$\frac{\partial \psi}{\partial y}\frac{\partial \omega_x}{\partial x} - \left(\frac{\partial \psi}{\partial x} + \frac{\partial \theta}{\partial z}\right)\frac{\partial \omega_x}{\partial y} + \frac{\partial \theta}{\partial y}\frac{\partial \omega_x}{\partial z} - \omega_x\frac{\partial u}{\partial x} - \omega_z\frac{\partial u}{\partial z} - \left(\frac{\partial u}{\partial z} - \frac{\partial w}{\partial x}\right)\frac{\partial u}{\partial y} - \frac{1}{Re}\left(\frac{\partial^2 \omega_x}{\partial x^2} + \frac{\partial^2 \omega_x}{\partial y^2} + \frac{\partial^2 \omega_x}{\partial z^2}\right) = 0 \tag{11}$$

The vorticity definitions given in Eq. (9) are rewritten in terms of the streamlike functions in Eqs. (6–8) to yield

$$\omega_z = -\frac{\partial^2 \psi}{\partial x^2} - \frac{\partial^2 \psi}{\partial y^2} - \frac{\partial^2 \theta}{\partial x \partial z} \tag{12}$$

$$\omega_x = \frac{\partial^2 \theta}{\partial y^2} + \frac{\partial^2 \theta}{\partial z^2} + \frac{\partial^2 \psi}{\partial x \partial z} \tag{13}$$

Equations (10–13) represent four equations in the four unknowns, ω_z, ω_x, ψ, and θ, which have been numerically solved in the present effort. In formulating these equations the v-velocity and the y-component of vorticity, $\omega_y = \partial u/\partial z - \partial w/\partial x$, have been eliminated through the use of their relationship to the other dependent variables. The u- and w-velocity components also have been eliminated by expressing them everywhere in terms of the streamlike functions. In addition, the "source terms" in Eqs. (10) and (11) that arise from the vorticity stretching term have been lagged in the current iterative procedure used to solve these equations. This point will be further discussed later in the Solution Procedure Section.

Using Eqs. (6) and (8) for the velocity field, the resulting pressure field may be determined through the solution of a Poisson equation, which results from cross differentiation of the primitive variable Navier-Stokes equations as described in Ref. 10. The resulting equation relating the pressure and velocity fields is given by

$$\nabla^2 p = -\left(\frac{\partial u}{\partial x}\right)^2 - \left(\frac{\partial v}{\partial y}\right)^2 - \left(\frac{\partial w}{\partial z}\right)^2 - 2\frac{\partial v}{\partial x}\frac{\partial u}{\partial y} - 2\frac{\partial w}{\partial x}\frac{\partial u}{\partial z} - 2\frac{\partial w}{\partial y}\frac{\partial v}{\partial z} \tag{14}$$

The governing equations given by Eqs. (6), (8), and (10–13) form the vorticity/streamlike function alternative to the full Navier-Stokes equations given in Eqs. (1) and (2). At this point, no approximations have been made other than to assume steady, incompressible, laminar flow. The present study has been limited to an analysis of external boundary-layer-like flows including separation in which the shear layers lay nearly parallel to the plane $y = 0$. Hence, for simplification, the vorticity diffusion terms in the x- and z-directions have been deleted, which leads to a set of equations often referred to as the "thin-layer" Navier-Stokes equations.

Boundary Conditions

A series of flow problems have been addressed in the present investigation that are shown schematically with the computational region in Fig. 1. The boundary conditions used at each of the boundaries for the viscous flow calculations presented in this paper will now be discussed. A similar set of boundary conditions for inviscid flow computations is described in Ref. 10.

At the upstream boundary, AEHD, the axial component u-velocity profile is specified as a function of the spanwise (z) position and is held fixed during iteration. For the calculations presented here, these axial component velocity profiles have been determined from a direct two-dimensional boundary-layer procedure[22] and held fixed in the spanwise direction. The normal and spanwise velocity components, v and w, were assumed to be zero along the upstream plane. Once the u-velocity profile is defined at the upstream boundary, the ψ streamlike function is calculated by integrating the profile in the normal (y) direction and the ω_z distribution is determined by differentiating the profile with respect to y. These boundary conditions are given by

$$u - \text{specified}, \qquad v = w = \omega_x = 0$$

$$\psi = \int_0^{y_{max}} u\,dy, \qquad \omega_z = -\frac{\partial u}{\partial y} \tag{15}$$

The x,y plane, ABCD, shown in Fig. 1 at the minimum z-location, has been assumed to be a plane of symmetry with respect to the z-direction. For this type of boundary, the values of w, ω_x, and θ are equal to zero as well as the derivatives of u, v, and ω_z with respect to z, which is written as

$$\theta = 0$$

$$w = 0, \quad \frac{\partial u}{\partial z} = \frac{\partial v}{\partial z} = 0$$

$$\omega_x = 0, \quad \frac{\partial \omega_z}{\partial z} = 0 \tag{16}$$

The lower z,y boundary, ABFE, is treated as a solid boundary where a zero velocity condition is imposed by setting the two streamlike functions, ψ and θ, as well as their derivatives with respect to y equal to zero. These conditions are given by

$$\psi = \theta = \frac{\partial \psi}{\partial y} = \frac{\partial \theta}{\partial y} = 0 \tag{17}$$

The Neumann boundary condition given in Eq. (17) is implemented using an additional computational node located one

grid spacing below the wall where the values of the streamlike functions are adjusted to satisfy Eq. (17). In addition to enforcing the zero velocity condition, this treatment of the Neumann condition (see Ref. 10) allows for the direct calculation of the vorticity at the wall as part of the implicit calculation. This application also removes the need for special one-sided differencing at the wall like that used by Briley[12] in order to satisfy the Poisson equations for the streamlike functions.

For the calculations presented in this paper, freestream boundary conditions were imposed at the upper z,y plane, DCGH, in Fig. 1 through the use of the following tangency conditions

$$\psi = \text{const}, \quad \theta = \text{const}$$

$$\omega_x = \omega_z = 0 \tag{18}$$

under the assumption that the DCGH boundary, which is located sufficiently far from the solid surface, represents a stream sheet. These conditions do not permit mass flow across this boundary and have been found to be superior to the Neumann conditions $u = \partial\psi/\partial y = 1$ and $w = \partial\theta/\partial y = 0$ for the highly stretched meshes used in the present calculations.

At the x far-field z,y plane, BFGC, the second derivatives of ψ, θ, u, and w with respect to x are set equal to zero. Similarly, the second derivatives of ψ, θ, u, and w with respect to z are set equal to zero at the z far-field x,y plane, EFGH. These conditions, which are consistent with the assumption of boundary-layer flows in the far field, are given as

$$\frac{\partial^2\psi}{\partial x^2} = \frac{\partial^2\theta}{\partial x^2} = \frac{\partial^2 u}{\partial x^2} = \frac{\partial^2 w}{\partial x^2} = 0 \quad \text{at } x \text{ far field}$$

$$\frac{\partial^2\psi}{\partial z^2} = \frac{\partial^2\theta}{\partial z^2} = \frac{\partial^2 u}{\partial z^2} = \frac{\partial^2 w}{\partial z^2} = 0 \quad \text{at } z \text{ far field} \tag{19}$$

In general, the vorticity/streamlike function analysis is not limited to these particular conditions at each boundary. Other boundary conditions could be easily substituted for each of the computational domain boundaries.

Solution Procedure

In the present analysis, the stretched and sheared computational grid in the physical (Cartesian) coordinate system is transformed into a uniformly spaced computational domain that exists between 0 and 1 in all three directions as explained in Ref. 10. Although a stretched/sheared mesh with locally varying mesh spacing is used in the physical Cartesian grid, a uniform mesh in each of the three directions is defined in the computational domain. This allows standard second-order accurate central difference formula to be used in the discretization of Eqs. (6), (8), and (10–13) with the exception of the axial and spanwise convection terms of the vorticity transport equations. For these convection terms, a first-order windward difference operator similar to that used for interacting boundary-layer calculations is used to model the parabolic nature of the vorticity transport equations. In addition, the streamwise derivative of ψ and the spanwise derivative of θ, which are both associated with the v-velocity component in the convection terms of the vorticity transport equations, are approximated with first-order backward and windward differences, respectively, as guided by interacting boundary-layer theory. Thus, in the inviscid region where the Poisson streamlike function equations dominate the flow, only central difference formulas are used to model the elliptic nature of the equations, whereas in the viscous region, which is dominated by the vorticity transport equations, appropriate one-sided windward differences are used to model the parabolic nature of these equations.

In the current investigation, a successive line relaxation technique along lines of x = const and z = const is used for the implicit solution of the governing equations. Since these lines along which the solution is determined are essentially perpendicular to the solid surface in a similar fashion as used by boundary-layer techniques, the governing equations given in Eqs. (6), (8), and (10–13) can be either solved simultaneously or partitioned into smaller equation sets by uncoupling the spanwise flow equations from the equations governing the axial flow. For three-dimensional external flows where the spanwise flow component is small relative to the axial flow as is the case for the problems in this investigation, Eqs. (6), (10), and (12) can be uncoupled from Eqs. (8), (11), and (13) and solved as two sets of 3×3 block tridiagonal equations. In this approach, ψ, ω_z, and u are solved simultaneously with θ, ω_x, and w lagged from the previous global iteration. Then θ, ω_x, and w are determined using the latest values of ψ, ω_z, and u. In order to simplify the solution procedure even further, the source terms in the vorticity transport equations, which are cast in terms of the u- and w-velocity components can be treated explicitly, thereby reducing the two uncoupled systems to each have two equations and two unknowns. This is the approach taken in the current investigation. In the future, solution of flows with strong spanwise/mainstream flow coupling may require an alternate treatment of the source terms in the transport equations, at which time three-dimensional boundary-layer theory can be used to identify the dominant source terms and provide guidance in their numerical treatment. Hence, in the current procedure, Eqs. (6), (10), and (12) are uncoupled from Eqs. (8), (11), and (13) with the u- and w-velocities lagged from the previous column iteration. This allows Eqs. (10) and (12) in addition to Eqs. (11) and (13) to be solved as two uncoupled systems of 2×2 block-tridiagonal equations. Each 2×2 system is solved implicitly using a Gauss-Seidel relaxation procedure. This line relaxation procedure consists of application of the upper boundary conditions, solution of the recursion coefficients from the upper boundary to the lower boundary, application of the lower solid wall boundary conditions, followed by backward substitution from the lower wall to the upper boundary to determine the changes in the streamlike functions and vorticity components. Column iteration may be used to eliminate the errors due to the nonlinearities and to increase stability of the global iteration procedure. Upon completion of each column iteration, the corresponding u- and w-velocity components are updated using Eqs. (6) and (8), respectively. An underrelaxation factor of 0.8 has been used on the vorticity transport equations for the calculation of the separated flow cases shown in this paper. Currently, the line relaxation scheme is marched in the spanwise (z) direction followed with a step in the axial (x) direction. Alternate marching and equation coupling strategies currently are being investigated.

Results and Discussion

The objective of the present research has been to demonstrate that converged, accurate solutions can be obtained from a streamlike function/vorticity transport approach for inviscid and viscous, laminar three-dimensional external flows. A series of two-dimensional and three-dimensional flow problems have been addressed in Ref. 10. Solutions for these cases have been compared to several well-documented numerical procedures including a finite-difference boundary-layer technique[22] for two-dimensional attached viscous flows, two-dimensional and three-dimensional interacting boundary-layer schemes[6,23,24] for separated viscous flows, and a two-dimensional stream function[23] or three-dimensional small disturbance procedure[6] for inviscid flows. In addition to the solutions given in Ref. 10, calculations for the viscous flow over a three-dimensional trough and bump will be discussed at this time. Limited computational grid refinement studies have been performed as part of the comparison of the present Navier-Stokes solutions with other numerical procedures. Further grid refinement studies are required, however, to determine the optimum computational grid densities that ensure accuracy and maximize computational efficiency.

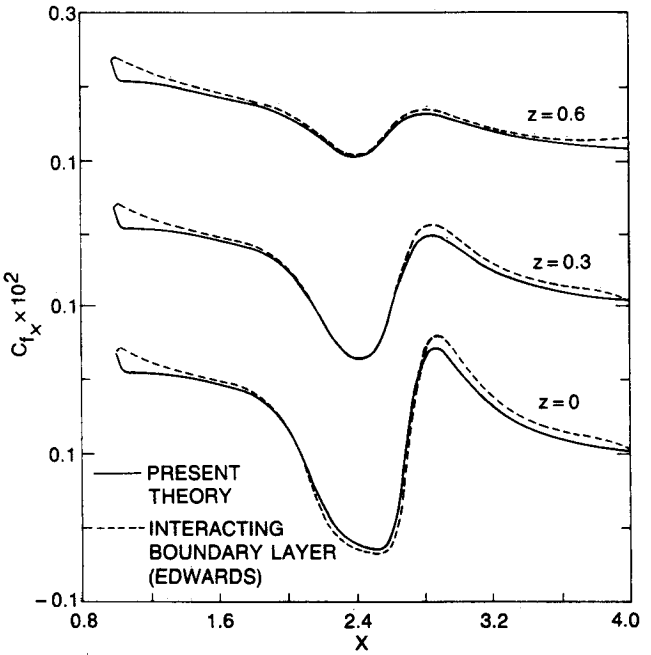

Fig. 2 Predicted axial component of skin friction for 3% trough, $Re = 8 \times 10^4$.

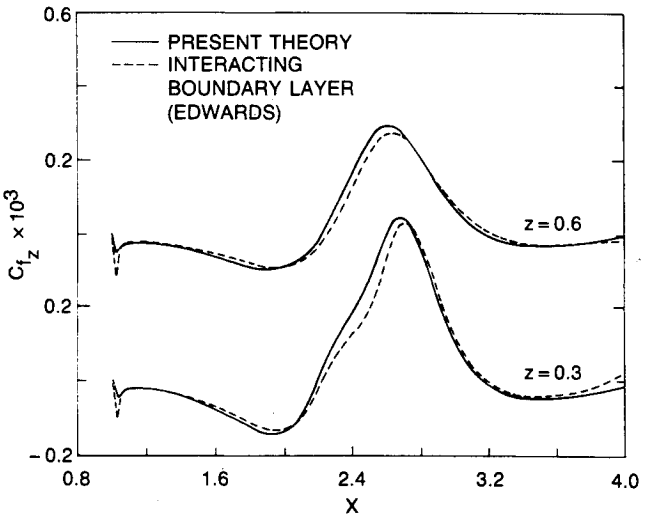

Fig. 3 Predicted spanwise component of skin friction for 3% trough, $Re = 8 \times 10^4$.

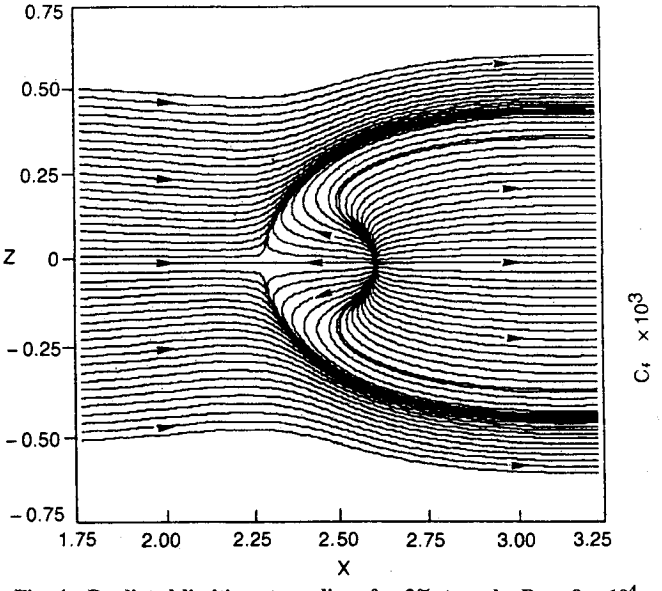

Fig. 4 Predicted limiting streamlines for 3% trough, $Re = 8 \times 10^4$.

Three-Dimensional Trough

A three-dimensional variation of the Carter-Wornom[24] trough geometry has been used in the current investigation where the present vorticity/streamlike function analysis has been compared in detail with the three-dimensional interacting boundary-layer calculations of Edwards.[6] The surface of the trough is described by the function

$$y(x,z) = -t \operatorname{sech}(4x - 10) \operatorname{sech}(4z) \qquad (20)$$

where t is the trough depth. A three-dimensional calculation was performed for a $t = 0.03$ trough at an upstream reference Reynolds number of 8×10^4. In this case, the flow separated at the bottom of the trough on the plane of symmetry. A 121-point uniform mesh was constructed in the x-direction between $x = 1.0$ and $x = 4.0$. In the z-direction, a 31-point uniform mesh was constructed between $z = 0.0$ and $z = 1.5$. The computational mesh was stretched in the y-direction from the lower surface to the outer boundary, located at $y = 5.0$, using 61 points with a minimal spacing of 5×10^{-4} at the wall, which guaranteed a minimum of 20 points in the boundary layer. The u-velocity profile used to define the upstream boundary conditions for the vorticity/streamlike function calculation was determined from a direct finite-difference boundary-layer calculation[22] extending from $x = 0.0$ (sharp leading edge) to $x = 1.0$. As described earlier, the v- and w-velocity components were assumed to be zero at the upstream boundary.

A comparison of the axial skin friction distribution with the three-dimensional interacting boundary-layer procedure of Edwards[6] at three different $z = \text{const}$ stations is shown in Fig. 2. The same computational grid distribution in the x,z plane was used for the interacting boundary-layer calculation as that used for the vorticity/streamlike function calculation. This figure shows that the present analysis is in very good agreement with the interacting boundary-layer calculation. The adverse streamwise pressure gradient located at the beginning of the trough causes the axial skin friction component to decrease. Separation of the flow occurs at the bottom of the trough on the plane of symmetry. Subsequent reattachment of the flow occurs downstream of the trough center on the plane of symmetry where the axial skin friction component rapidly rises to a maximum downstream of which the flow returns to that over a two-dimensional flat plate. Both solutions approach two-dimensional flat plate flow at the z far field.

A comparison between the predictions of the vorticity based Navier-Stokes analysis and the interacting boundary-layer procedure of Edwards[6] for the spanwise skin friction component is shown in Fig. 3 at different z-planes. Good agreement also exists between the two solutions for the spanwise skin friction component with only minor differences existing between the solutions near the plane of symmetry. Upstream of the trough center, the flow migrates toward the plane of symmetry until the favorable spanwise pressure gradients force the flow to change direction and travel outward in the positive z direction. As the flow emerges from the center of the trough, the adverse spanwise pressure gradient turns the flow back toward the plane of symmetry where it returns to two-dimensional flow. At the z far field, the flow remains two-dimensional over the entire axial length of the trough. Small local oscillations in the spanwise skin friction component occur at the upstream boundary due to the two-dimensional assumption that the v- and w-velocities are zero at this boundary. These oscillations are quickly eliminated away from the inlet boundary, however. The interacting boundary-layer solution predicts a small plateau in the spanwise skin friction near the plane of symmetry at $x = 2.4$ whereas the vorticity/streamlike function procedure does not. This minor difference is perhaps due to an inadequate computational grid in the Navier-Stokes calculation. A similar skin friction distribution was observed for a

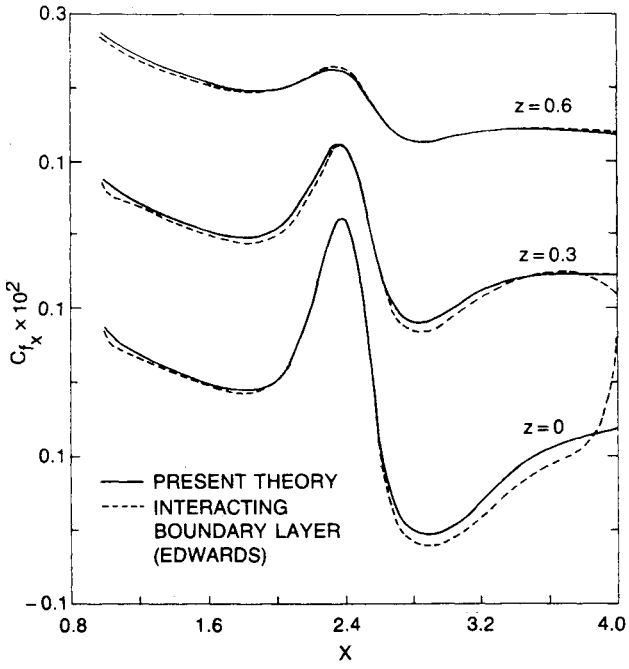

Fig. 5 Predicted axial component of skin friction for 3% bump, $Re = 6 \times 10^4$.

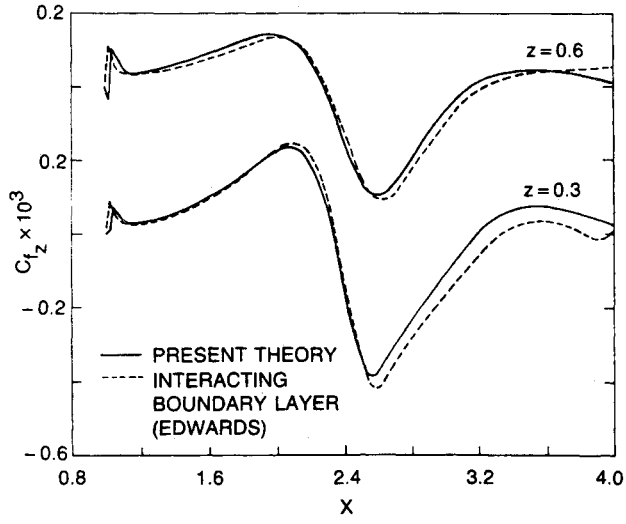

Fig. 6 Predicted spanwise component of skin friction for 3% bump, $Re = 6 \times 10^4$.

lower Reynolds number trough case shown in Ref. 10 in which the Navier-Stokes analysis was able to resolve this detail. A similar C_{f_z} skin friction distribution was predicted by Duck and Burggraf[25] for laminar, incompressible flow over a three-dimensional trough at an infinite Reynolds number using triple deck theory.

The extent of the reversed axial flow region for this case is dramatically shown in Fig. 4 with a plot of the limiting streamlines. Figure 4 shows that even though the geometry is simple in nature, the resulting flowfield is rather complex. The flow along the plane of symmetry separates at the saddle point located at $x = 2.28$. Reattachment of the flow occurs at the nodal point located on the plane of symmetry at $x = 2.61$. The surface flow away from the plane of symmetry is forced around the reversed axial flow region along a line of coalescing streamlines, which is often referred to as a dividing streamline. The region between the dividing streamlines defines a "corridor" that cannot be penetrated by the upstream surface flow. All of the streamlines inside the corridor originate from the nodal point. A region of reversed axial flow exists between the saddle and nodal points extending outward in the z-direction to $z = 0.19$. The surface flow in this reversed axial flow region migrates away from the plane of symmetry due to the spanwise pressure gradients, where it eventually turns back toward the positive x-direction and travels parallel to the main stream.

Three-Dimensional Bump

A three-dimensional vorticity/streamlike function calculation also has been performed for the viscous flow over a three-dimensional bump at an upstream reference Reynolds number of 6×10^4. The bump geometry was determined from Eq. (20) with a bump height, $t = -0.03$. The flow separated at the aft end of the bump on the plane of symmetry. The same computational grid distribution was used for this case as that for the trough case previously described. The u-velocity profile used to define the upstream boundary conditions for the Navier-Stokes calculation was found from a direct finite-difference boundary-layer calculation[22] extending from $x = 0.0$ (sharp leading edge) to $x = 1.0$. The v- and w-velocity components again were assumed to be zero at the upstream boundary.

Comparison of the axial skin friction distribution predicted by the present analysis and the interacting boundary-layer procedure of Edwards[6] at three $z = \text{const}$ stations is shown in Fig. 5. The interacting boundary-layer calculation used the same computational grid distribution in the x,z plane as used for the present Navier-Stokes analysis. Figure 5 shows that the present analysis is in very good agreement with the interacting boundary-layer calculation. In this case, C_{f_x} rises to a maximum as the flow accelerates over the bump. As the flow begins to decelerate behind the center of the bump, the axial skin friction quickly decreases and separation occurs at the plane of symmetry. The flow reattaches somewhat downstream of the bump at the plane of symmetry and quickly returns to flat plate flow. The interacting boundary-layer solution shown in Fig. 5 has a sudden shift in the C_{f_x} distribution at the x far-field boundary near the plane of symmetry whereas the Navier-Stokes solution does not. The shift in the interacting boundary-layer solution at this location is caused by an omission of the effective displacement surface effects from outside of the computational domain in the inviscid analysis which consists of a three-dimensional Cauchy integral procedure. This problem could be eliminated by placement of the x far-field boundary at a position further downstream of the bump. The discrepancy between the two solutions disappears as the z far-field boundary is approached, with both techniques essentially producing a two-dimensional flat plate flow solution. Also, the extent of the reversed axial flow region predicted by the Navier-Stokes procedure is somewhat smaller (i.e., from $x = 2.8$ to $x = 3.0$) as compared to that predicted with the interacting boundary-layer calculation (i.e., from $x = 2.7$ to $x = 3.1$). This difference possibly may be eliminated by using a finer grid distribution in the Navier-Stokes calculation.

A comparison between the two predictions of the spanwise skin friction component is shown in Fig. 6 where C_{f_z} is plotted at different z-planes. Good agreement exists between the two solutions for the spanwise skin friction component with only slight differences existing at the end of the bump near the plane of symmetry. The spanwise flow for the bump is somewhat opposite to that for the previously described trough case. As the flow approaches the bump center near the plane of symmetry, the spanwise pressure gradients drive the flow outward in the positive z-direction and then inward toward the plane of symmetry. Downstream of the bump center, the flow again moves outward and then returns to two-dimensional flow at the exit boundary. As shown in Fig. 6, the solution of the vorticity/streamlike function approach is nearly uniform at the x far-field boundary, whereas the interacting boundary-layer calculation shows some fluctuation in C_{f_z} at this location similar to that shown in Fig. 5. Both techniques approach a two-dimensional flat plate solution at the z far-field.

A plot of the limiting streamlines for this case is shown in Fig. 7. This figure has many of the same features shown in Fig. 4 for the trough case but yet is different in structure. In

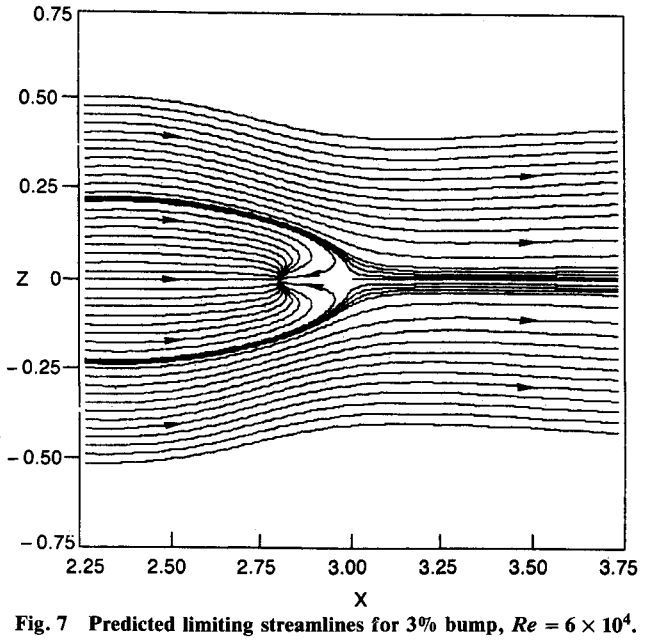

Fig. 7 Predicted limiting streamlines for 3% bump, $Re = 6 \times 10^4$.

this case, a nodal point is located at the separation point on the plane of symmetry at $x = 2.8$. A saddle point exists at the reattachment point located on the plane of symmetry at $x = 3.0$. The dividing streamline caused by the flow separation begins at the upstream boundary and merges toward the plane of symmetry at the saddle point where it then travels downstream along the plane of symmetry. In this case, the "corridor" caused by the separation is located upstream of the disturbance. The streamlines inside this corridor terminate at the nodal point where the flow separates from the surface. A region of reversed axial flow exists between the nodal and saddle points extending in the spanwise direction to $z = 0.07$. The surface flow outside of the corridor is attached and moves downstream around the bump and the flow inside the corridor.

Three-Dimensional Swept Trough

In general, flows over aerodynamic surfaces are not necessarily dominated by a vorticity component that aligns itself with either the x- or z-directions as shown for the previous cases where the axial vorticity component ω_x was relatively small compared to the spanwise vorticity component ω_z. For example, the flowfield at a wing tip exhibits strong interaction between the axial and spanwise vorticity components. As part of the present study, a brief investigation into separated viscous flows with strong coupling between the axial and spanwise vorticity components was performed to demonstrate the applicability of the current numerical procedure to flows such as these. In particular, the focus of this investigation was to demonstrate the stability of the current numerical approach that uncouples the governing equations for the spanwise flow from the axial flow equations for flows with strong axial/spanwise flow interaction. This demonstration has been accomplished in the current study by sweeping the three-dimensional trough geometry given in Eq. (20) 45 deg to the mainstream flow resulting in a spanwise flow component with the same magnitude as the axial flow component. Likewise, the axial vorticity in the flow was similar in magnitude to the spanwise vorticity component. As in the previous three-dimensional trough calculation, this case was calculated for an upstream reference Reynolds of 8×10^4. An 81×41 point uniform grid distribution was used in the x- and z-directions, respectively, between $1.0 < x < 4.0$ and $-1.5 < z < 1.5$. The computational mesh in the x- and z-directions were aligned perpendicular and parallel to the leading edge of the swept plate. The computational mesh was stretched in the y-direction between the lower surface and the outer boundary, located at $y = 5.0$, using 61 points with a minimal spacing of 5×10^{-4} at the wall. A

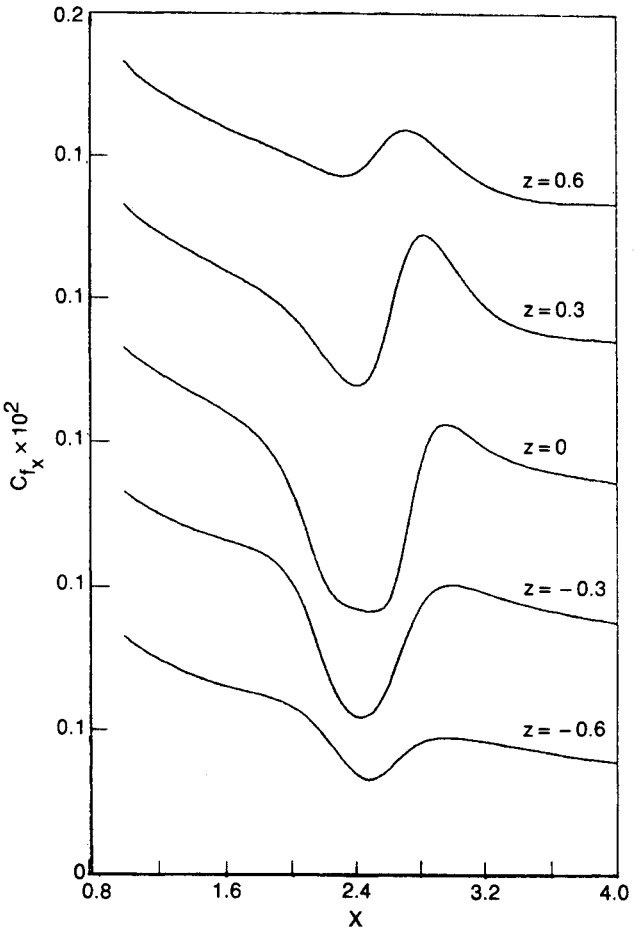

Fig. 8 Predicted axial component of skin friction for 3% swept trough, $Re = 8 \times 10^4$.

finite-difference boundary-layer calculation for an infinite swept flat plate[22] extending from the leading edge (sharp) located at $x = 0.0$ to $x = 4.0$ was used to obtain the u- and w-velocity profiles at the $x = 1.0$ and along the $z = -1.5$ planes. The boundary conditions given in Eq. (15) were substituted for the plane of symmetry conditions at the $z = -1.5$ plane with the exception that the w-velocity and the axial vorticity ω_x were no longer zero. In addition to these boundary conditions, the axial vorticity distribution in this plane was determined by differentiating the w-velocity profile with respect to y and the spanwise streamlike function θ was calculated by integrating the w-velocity profile in the y-direction. The conditions at the $x = 0.0$ and along the $z = -1.5$ planes were held fixed during the calculation.

This calculation converged similarly to the previous trough and bump cases with no sign of stability problems demonstrating that the current equation coupling strategy is a viable technique even for flows where the x- and z-vorticity components are of the same magnitude. Further studies are necessary, however, to determine if instabilities occur with refinements in the computational grid. In addition, further calculations on grids with finer mesh spacing are required to determine if the existing solution is grid independent.

Figures 8 and 9 show the predicted axial (C_{f_x}) and spanwise (C_{f_z}) skin friction components at five different $z = \text{const}$ planes. These figures show that the axial vorticity indicated by the C_{f_z} skin friction plot is roughly the same magnitude as the spanwise vorticity, which is proportional to C_{f_x}. These figures also show that the predicted solution is smooth and free of oscillations. Future work will be directed at comparison between the present Navier-Stokes analysis and interacting boundary-layer theory for cases such as this where the axial and spanwise flow components are closely coupled.

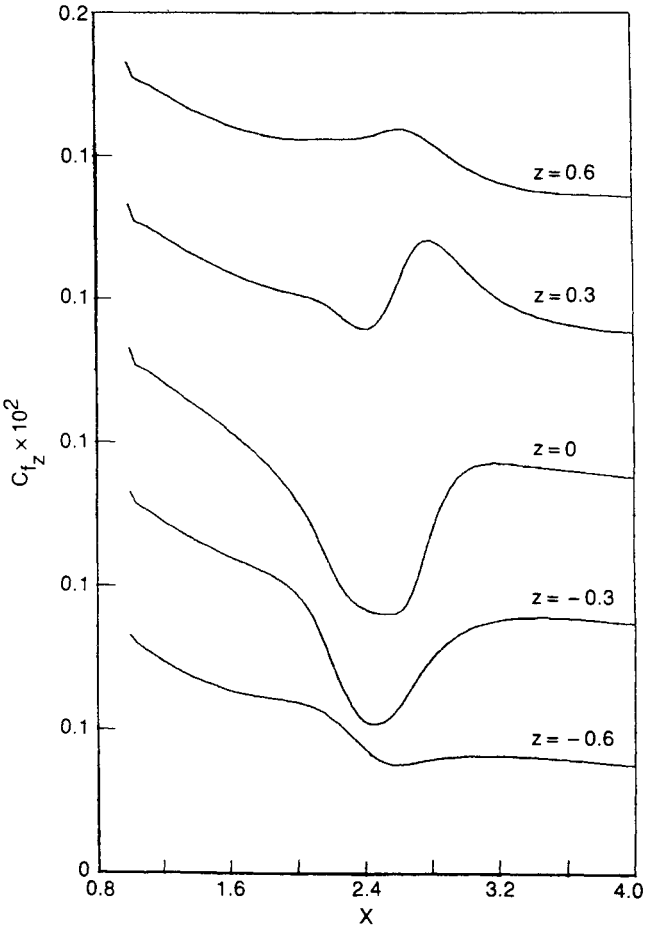

Fig. 9 Predicted spanwise component of skin friction for 3% swept trough, $Re = 8 \times 10^4$.

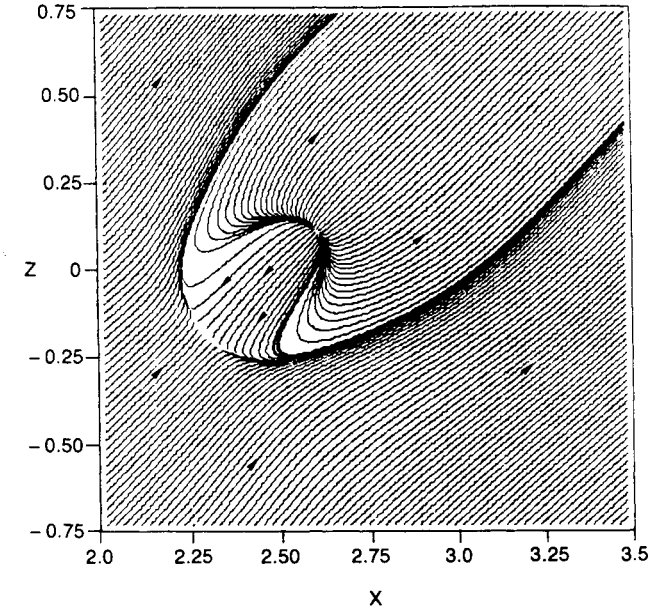

Fig. 10 Predicted limiting streamlines for 3% swept trough, $Re = 8 \times 10^4$.

Figure 10 shows the limiting streamlines predicted for this case. This figure shows the same type of flow features as those shown in Fig. 4 for the previous trough case. A saddle point exists at the separation point that is located at $x = 2.31$, $z = -0.19$. A region of reversed axial and spanwise flow exists between the saddle point and the reattachment (nodal) point located at $x = 2.62$, $z = 0.11$. Both the saddle and nodal points lie in a geometrical plane of symmetry that is 45 deg relative to the x- and z-directions passing through the center of the trough and aligned with the mainstream flow direction. Figure 10 shows that the predicted limiting streamlines are symmetric about this plane.

Figures 2–10 show that the present Navier-Stokes approach is capable of accurately predicting the complex flow structure resulting from separated flow. Although the model problems shown in these figures correspond to simple geometries, the flow structure resulting from separation produces rather large gradients in each of the three flow directions. These calculations provide strong encouragement that the present vorticity-based approach to solving the Navier-Stokes equations can be applied successfully to aerodynamic flows that are three-dimensional vortex dominated.

Concluding Remarks

A three-dimensional streamlike function/vorticity transport procedure has been developed for the analysis of two- and three-dimensional inviscid and viscous external flows. A detailed discussion is presented that demonstrates that this approach incorporates many of the features of interacting boundary-layer theory for strongly interacting viscous and inviscid flows. Numerical techniques have been applied to the present Navier-Stokes formulation that honor the elliptic nature of the problem in the inviscid region of flow and the parabolic nature in the viscous part of the flow. The principal focus of the present investigation was to demonstrate the feasibility of this three-dimensional streamlike function/vorticity approach to obtain converged, accurate solutions for both inviscid and viscous external flows. This goal has been pursued through the numerical study of a series of two-dimensional and three-dimensional model problems. For the three-dimensional problems in this study, it was found sufficient to uncouple the mainstream and crossflow solutions that, through the use of an implicit line relaxation scheme, resulted in a set of 2×2 block-tridiagonal equations for each of the respective directions at each computational station on the body surface. Overall, agreement with other comparable numerical solutions has been found to be quite favorable, which leads to the principal conclusion of this research that this new vorticity/streamlike function technique is capable of yielding solutions that simultaneously capture the details of the inviscid and viscous flow regions.

The calculations shown in this paper for the Navier-Stokes technique took approximately 3 s per global iteration on $121 \times 61 \times 31$ grids using a Cray X-MP. Convergence occurred in these calculations between 1000–3000 global iterations with a four-orders-in-magnitude reduction in the streamlike function and vorticity residuals. The computational time for the Navier-Stokes calculations was roughly an order of magnitude greater than that for the three-dimensional interaction procedure. Computational times of the Navier-Stokes technique may be reduced in the future, however, with the addition of convergence acceleration techniques such as a multiple-grid algorithm. In addition, future work on this approach will include investigations of alternate marching and equation coupling strategies to improve vectorization and to allow multitasking of the procedure for increased computational efficiency.

Acknowledgments

This research effort was supported by the Air Force Office of Scientific Research under Contract F49620-84-C-0032 and by the United Technologies Research Center under the corporate research program. The authors would like to thank Mr. D. E. Edwards for his helpful discussions about the interacting boundary-layer calculations. The authors also thank Cray Research, Inc., for use of their Cray X-MP and Dr. Charles Finan of Cray Research, Inc., for vectorization of the three-dimensional vorticity/streamlike function approach and for providing the solutions presented in this paper.

References

[1]LeBalleur, J. C., "Couplage Visqueux-non Visqueux: Methode Numerique et Applications Aux Ecoulements Bidimensionnels Transsoniques et Supersoniques, *La Recherche Aerospatialte,* No. 1978-2, 1978, pp. 65–76.

[2]Carter, J. E., "A New Boundary-Layer Inviscid Iteration Technique for Separated Flow," AIAA Paper 79-1450, July 1979.

[3]Veldman, A. E. P., A Numerical View on Strong Viscous-Inviscid Interaction, NLR MP 83048 U, 1978.

[4]McDonald, H. and Briley, W. R., "A Survey of Recent Work on Interacted Boundary Layer Theory for Flow with Separation," Second Symposium on Numerical and Physical Aspects of Aerodynamic Flows, Long Beach, CA, Jan. 1985.

[5]Edwards, D. and Carter, J., "Analysis of Three-Dimensional Separated Flow with the Boundary-Layer Equations," AIAA Paper 85-1499, July 1985.

[6]Edwards, D., "Analysis of 3-D Separated Flow Using Interacting Boundary-Layer Theory," IUTAM Symposium on Boundary Layer Separation, London, England, Aug. 1986.

[7]Chen, Z. L. and Wu, J. M., "Approximate Viscous/Inviscid Interacting Method for Laminar and Turbulent Flows with Separation," AIAA Paper 84-0267, Jan. 1984.

[8]Steger, J. L. and van Dalsem, W. R., "Developments in the Simulation of Separated Flows Using Finite Difference Methods," Third Symposium on Numerical and Physical Aspects of Aerodynamic Flows, Long Beach, CA, Jan. 1985.

[9]Whitfield, D. L., "Viscous-Inviscid Interaction Computations Using a Pseudo Navier-Stokes Approach," Third Symposium on Numerical and Physical Aspects of Aerodynamic Flows, Long Beach, CA, Jan. 1985.

[10]Davis, R. L., Carter, J. E., and Hafez, M., "Three-Dimensional Viscous Flow Solutions with a Vorticity-Stream Function Formulation," Air Force Office of Scientific Research, AFOSR-TR-86, May 1986.

[11]Werle, M. J. and Bernstein, J. M., "A Comparative Numerical Study of Models of the Navier-Stokes Equations for Incompressible Separated Flows," AIAA Paper 74-48, Jan. 1985.

[12]Briley, W. R., "A Numerical Study of Laminar Separation Bubbles Using the Navier-Stokes Equations," *Journal of Fluid Mechanics,* Vol. 47, 1971, pp. 713–736.

[13]Ghia, U. and Davis, R. T., "Solution of Navier-Stokes Equations for Flow Past a Class of Two Dimensional Semi-Infinite Bodies," AIAA Paper 74-12, 1974.

[14]Halim, A. and Hafez, M., "Calculation of Separation Bubbles Using Boundary-Layer-Type Equations—Part I & II," AIAA Paper 84-1585, June 1984.

[15]Hamed, A. and Abdallah, S., "Internal Three-Dimensional Viscous Flow Solution Using the Streamlike Function," *ASME Journal of Fluid Engineering,* Vol. 108, No. 3, Sept. 1986, pp. 348–353.

[16]Aziz, K. and Hellums, J., "Numerical Solution of the Three-Dimensional Equations of Motion for Laminar Natural Convection," *Physics of Fluids,* Vol. 10, 1967, pp. 314–324.

[17]Wong, A. K. and Reizes, J. A., "An Effective Vorticity-Vector Potential Formulation for the Numerical Solution of Three-Dimensional Duct Flow Problems," *Journal of Computational Physics,* Vol. 55, 1984, pp. 98–114.

[18]Aregbesola, Y. A. and Burley, D. M., "The Vector and Scalar Potential Method for the Numerical Solution of the Two- and Three-Dimensional Navier-Stokes Equations," *Journal of Computational Physics,* Vol. 24, 1977, pp. 398–415.

[19]Yang, H. and Camarero, R., "An Improved Vorticity-Potential Method for Three-Dimensional Duct Flow Simulations," *International Journal of Numerical Methods in Fluids,* Vol. 6, 1986, pp. 35–45.

[20]Lighthill, M. J., "Introduction. Boundary Layer Theory," *Laminar Boundary Layers,* edited by L. Rosenhead, Fluid Motion Memoirs, Oxford University Press, 1963, pp. 46–113.

[21]Lighthill, M. J., "On Displacement Thickness," *Journal of Fluid Mechanics,* Vol. 4, 1958, pp. 383–392.

[22]Carter, J. E, "Inverse Boundary-Layer Theory and Comparison with Experiment," NASA TP-1208, Sept. 1978.

[23]Edwards, D. and Carter, J., "A Quasi-Simultaneous Finite Difference Approach for Strongly Interacting Flow," Third Symposium on Numerical and Physical Aspects of Aerodynamic Flows, Long Beach, CA, Jan. 1985.

[24]Carter, J. and Wornom, S., "Solution for Incompressible Separated Boundary Layers Including Viscous-Inviscid Interaction," NASA SP-347, 1975.

[25]Duck, P. W. and Burggraf, O. R., "Spectral Solutions for Three-Dimensional Triple-Deck Flow Over Surface Topography," *Journal of Fluid Mechanics,* Vol. 162, 1986, pp. 1–22.